2

Physical metallurgy of aluminium alloys

Although most metals will alloy with aluminium, comparatively few have sufficient solid solubility to serve as major alloying additions. Of the commonly used elements, only zinc, magnesium (both greater than 10 atomic %)†, copper and silicon have significant solubilities (Table 2.1). However, several other elements with solubilities below 1 atomic % confer important improvements to alloy properties. Examples are some of the transition metals, e.g. chromium, manganese and zirconium, which are used primarily to form compounds that control grain structure. With the exception of hydrogen, elemental gases have no detectable solubility in either liquid or solid aluminium. Apart from tin, which is sparingly soluble, maximum soild solubility in binary

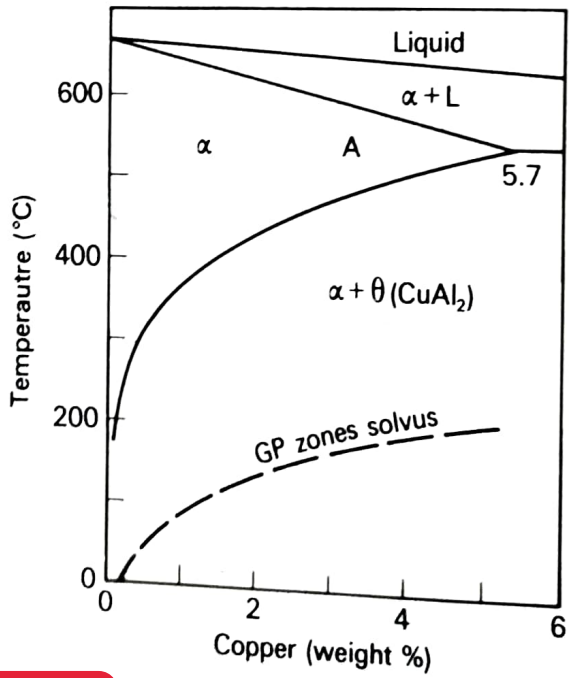

Fig. 2.1 Section of Al–Cu eutectic phase diagram. The position of GP zones solvus is also shown

† Unless stated otherwise, alloy compositions and additons are quoted in weight percentages.

Table 2.1 Solid solubility of elements in aluminium (from Van Horn, K.R. (Ed), *Aluminium*, Volume 1, American Society for Metals, Cleveland, Ohio,1967; Mondolfo, L.F., *Aluminium Alloys: Structure and Properties*, Butterworths, London, 1976)

Element	Temperature (°C)	Maximum solid solubility	
		(wt%)	(at%)
Cadmium	649	0.4	0.09
Cobalt	657	<0.02	<0.01
Copper	548	5.65	2.40
Chromium	661	0.77	0.40
Germanium	424	7.2	2.7
Iron	655	0.05	0.025
Lithium	600	4.2	16.3
Magnesium	450	17.4	18.5
Manganese	658	1.82	0.90
Nickel	640	0.04	0.02
Silicon	577	1.65	1.59
Silver	566	55.6	13.8
Tin	228	~0.06	~0.01
Titanium	665	~1.3	~0.74
Vanadium	661	~0.4	~0.21
Zinc	443	70	28.8
Zirconium	660.5	0.28	0.08

Note:
(i) Maximum solid solubility occurs at eutectic temperatures for all elements except chromium, titanium, vanadium, zinc and zirconium for which it occurs at peritectic temperatures.
(ii) Solid solubility at 20°C is estimated to be approximately 2 wt% for magnesium and zinc, 0.1–0.2 wt% for germanium, lithium and silver and below 0.1% for all other elements.

aluminium alloys occurs at eutectic and peritectic temperatures. Sections of typical eutectic and peritectic binary phase diagrams are shown in Figs 2.1 and 2.2.

High-purity aluminium in the annealed condition has very low yield strength (7–11 MPa). When it is desired to use annealed material, strength may be increased only by solid solution hardening. For this to be achieved, the solute must have appreciable solid solubility at the annealing temperature, must remain in solution after a slow cool, and must not be removed by reacting with other elements to form insoluble phases.

Figure 2.3 shows the increment in yield strength that occurs when selected solutes are added to high-purity aluminium. Some elements are shown in concentrations beyond their room temperature solubility but each alloy was processed to retain all the solute in solution. On an

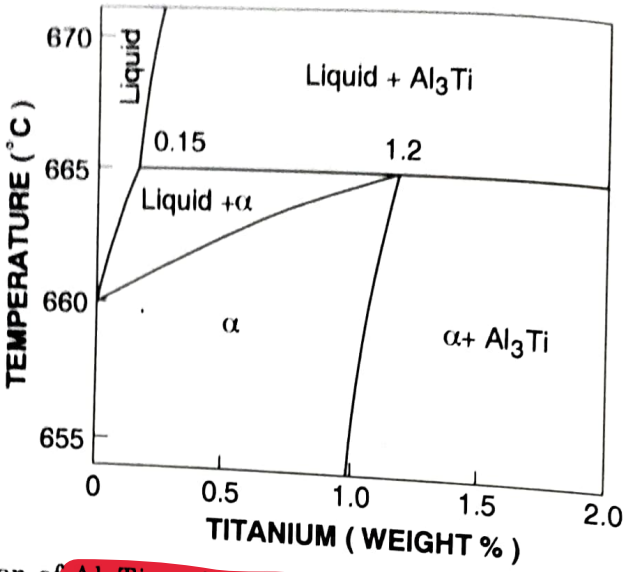

Fig. 2.2 Section of Al–Ti peritectic phase diagram

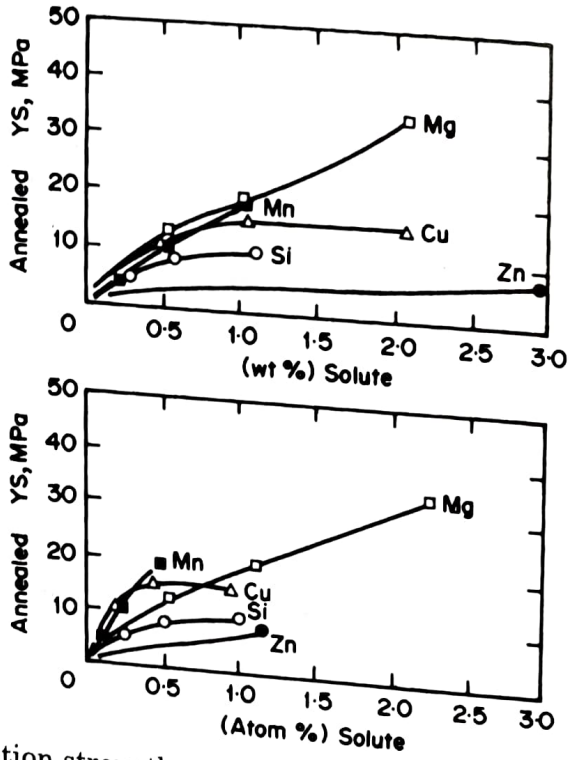

Fig. 2.3 Solid solution strengthening of high-purity binary aluminium alloys (from Sanders, R. E. *et al.*, *Proceedings of International Conference on Aluminium Alloys—Physical and Mechanical Properties*, Charlottesville, Virginia, Engineering Materials Advisory Services, Warley, U.K., 1941, 1986)

atomic basis, manganese and copper are the most effective strengtheners at 0.5% or less. However, manganese usually precipitates as the dispersoid Al_6Mn during ingot preheating (Section 3.1.4) and hot processing so that only 0.2–0.3% tends to remain in solution. Copper additions to the non-heat-treatable alloys are normally held to a

maximum of 0.3% to avoid possible formation of insoluble Al–Cu–Fe constituents. Magnesium is the most effective strengthener on a weight basis because of its relatively high solubility and annealed sheet and plate containing up to 6% of this element have yield strengths up to 175 MPa. It will also be noted that zinc, too, has a high solubility but causes very little strengthening.

Very high strength:weight ratios can be achieved in certain alloys because they show a marked response to age- or precipitation-hardening. Thus it is desirable to present a brief review of the essential principles associated with this phenomenon before considering specific alloy systems. These remarks also apply generally to those magnesium and titanium alloys in which precipitation occurs.

2.1 Principles of age-hardening

2.1.1 Decomposition of supersaturated solid solutions

The basic requirement for an alloy to be amenable to age-hardening is a decrease in solid solubility of one or more of the alloying elements with decreasing temperature. Heat treatment normally involves the following stages:

1. Solution treatment at a relatively high temperature within the single-phase region, e.g. A in Fig. 2.1, to dissolve the alloying elements.
2. Rapid cooling or quenching, usually to room temperature, to obtain a supersaturated solid solution (SSSS) of these elements in aluminium.
3. Controlled decomposition of the SSSS to form a finely dispersed precipitate, usually by ageing for convenient times at one and sometimes two intermediate temperatures.

The complete decomposition of an SSSS is usually a complex process which may involve several stages. Typically, Guinier–Preston (GP) zones and an intermediate precipitate may be formed in addition to the equilibrium phase. The GP zones are ordered, solute-rich clusters of atoms which may be only one or two atom planes in thickness. They retain the structure of the matrix and are coherent with it, although they usually produce appreciable elastic strains (Fig. 2.4). Their formation requires movements of atoms over relatively short distances so that they are very finely dispersed in the matrix with densities which may be as high as 10^{17} to 10^{18} cm^{-3}. Depending upon the alloy system, the rate of nucleation and the actual structure

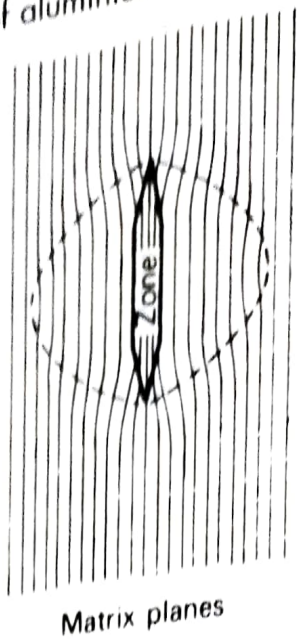

Fig. 2.4 Representation of the distortion of matrix lattice planes near to the coherent GP zone (from Nicholson, R. B. *et al.*, *J. Inst. Metals*, **87**, 429, 1958–59)

may be greatly influenced by the presence of excess vacant lattice sites that are also retained by quenching.

The intermediate precipitate is normally much larger in size than a GP zone and is only partly coherent with the lattice planes of the matrix. It has a definite composition and crystal structure which may differ only slightly from those of the equilibrium precipitate. In some alloys, the intermediate precipitate may be nucleated from, or at, the sites of stable GP zones. In others this phase nucleates heterogeneously at lattice defects such as dislocations (Fig. 2.5). Formation of the final equilibrium precipitate involves complete loss of coherency with the parent lattice. It forms only at relatively high ageing temperatures and, because it is coarsely dispersed, little hardening results.

Maximum hardening in commercial alloys occurs when there is present a critical dispersion of GP zones, or an intermediate precipitate, or both. In some cases the alloys are cold worked (e.g. by stretching 5%) after quenching and before ageing, which increases dislocation density and provides more sites at which heterogeneous nucleation of intermediate precipitates may occur.

2.1.2 The GP zones solvus

An important concept is that of the GP zones solvus which may be shown as a metastable line in the equilibrium diagram (Fig. 2.1). It defines the upper temperature limit of stability of the GP zones for different compositions although its precise location can vary depending upon the concentration of excess vacancies. Solvus lines can also

Fig. 2.5 Transmission electron micrograph showing the rods of the S-phase (Al_2CuMg) precipitated heterogeneously on dislocation lines. The alloy is Al–2.5Cu–1.5Mg, aged 7 h at 200°C (from Vietz, J. T. and Polmear, I. J., *J. Inst. Metals*, **94**, 410, 1966)

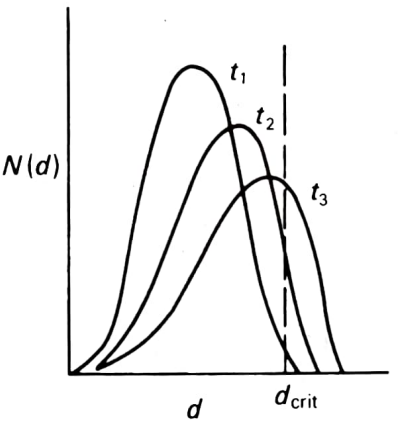

Fig. 2.6 Representation of the variation in GP zone size distribution with ageing time ($t_1 < t_2 < t_3$) (from Lorimer, G. W. and Nicholson, R. B., *The Mechanism of Phase Transformations in Crystalline Solids*, Institute of Metals, London, 1969)

be determined for other metastable precipitates. The distribution of GP zones sizes with ageing time is shown schematically in Fig. 2.6. There is strong experimental support for the model proposed by Lorimer and Nicholson whereby GP zones formed below the GP zones solvus temperature can act as nuclei for the next stage in the ageing process, usually the intermediate precipitate, providing they have reached a critical size (d_{crit} in Fig. 2.6). On the basis of this model, alloys have been classified into three types.

1. Alloys for which the quench-bath temperature and the ageing temperature are both above the GP zones solvus. Such alloys

show little or no response to age-hardening due to the difficulty of nucleating a finely dispersed precipitate. An example is the Al–Mg system in which quenching results in a very high level of supersaturation, but where hardening is absent in compositions containing less than 5–6% magnesium.

2. Alloys in which both the quench-bath and ageing temperatures are below the GP zones solvus, e.g. some Al–Mg–Si alloys.

3. Alloys in which the GP zones solvus lies between the quench-bath temperature and the ageing temperature. This situation is applicable in most age-hardenable aluminium alloys. Advantage may be taken of the nucleation of an intermediate precipitate from pre-existing GP zones of sizes above d_{crit} using two-stage or duplex ageing treatments. These are now applied to some alloys to improve certain properties and this is discussed in more detail in Section 3.5.5. They are particularly relevant with respect to the problem of stress-corrosion cracking in high-strength aluminium alloys.

2.1.3 Precipitate-free zones at grain boundaries

All alloys in which precipitation occurs have zones adjacent to grain boundaries which are depleted of precipitate and Fig. 2.7a shows comparatively wide zones in an aged, high-purity Al–Zn–Mg alloy. These precipitate-free zones (PFZs) are formed for two reasons. First, there is a narrow (~ 50 nm) region either side of a grain boundary which is depleted of solute due to the ready diffusion of solute atoms into the boundary where relatively large particles of precipitate are subsequently formed. Second, the remainder of a PFZ arises because of a depletion of vacancies to levels below that needed to assist with nucleation of precipitates at the particular ageing temperature. It has been proposed that the distribution of vacancies near a grain boundary can take the form shown schematically in Fig. 2.8 (curve A) and that a critical concentration C_1 is needed before nucleation of the precipitate can occur at temperature T_1. The width of the PFZ can be altered by heat treatment conditions; the zones are narrower for higher solution treatment temperatures and faster quenching rates, both of which increase the excess vacancy content (e.g. curve B in Fig. 2.8), and for lower ageing temperatures. This latter effect has been attributed to a higher concentration of solute which means that smaller nuclei will be stable, thereby reducing the critical vacancy concentration required for nucleation to occur (C_2 in Fig. 2.8). However, the vacancy-depleted part of a PFZ may be absent in some alloys aged at temperatures below the GP zones

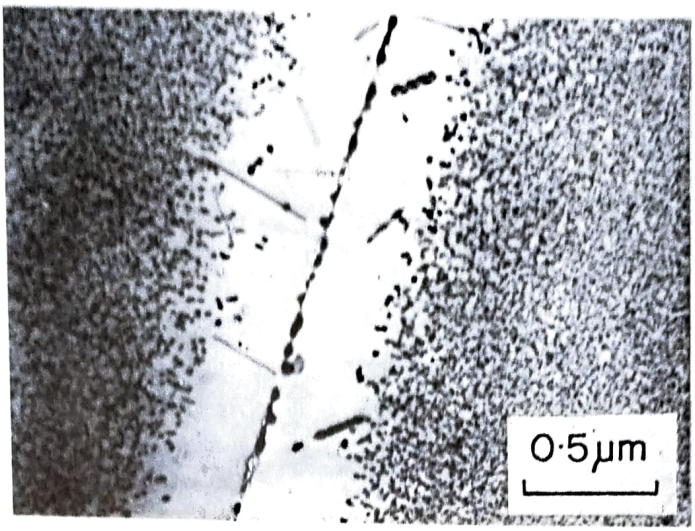

(a)

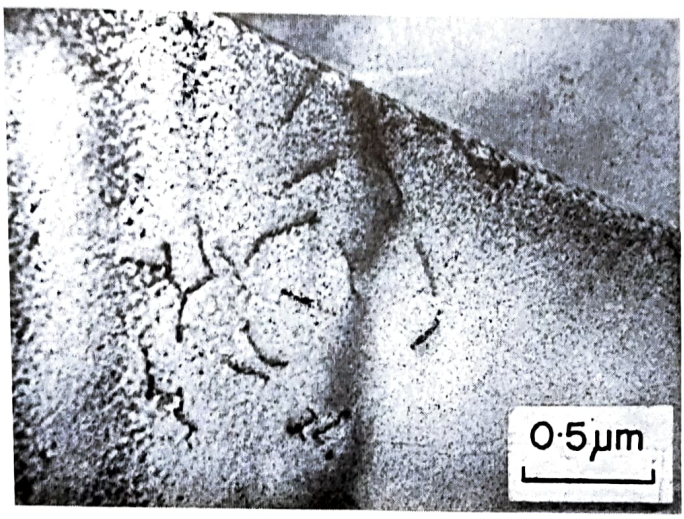

(b)

Fig. 2.7 (a) Wide PFZs in the alloy Al–4Zn–3Mg, aged 24 h at 150°C; (b) effect of 0.3% silver on PFZ width and precipitate distribution in Al–4Zn–3Mg, aged 24 h at 150°C (from Polmear, I. J., *J. Australian Inst. Met.* **17**, 1, 1972)

solvus as GP zones can form homogeneously without the need of vacancies.

2.1.4 Trace element effects

In common with other nucleation and growth processes, precipitation reactions may be greatly influenced by the presence of minor amounts or traces of certain elements. These changes can arise for a number of reasons including:

1. Preferential interaction with vacancies which reduces the rate of nucleation of GP zones.

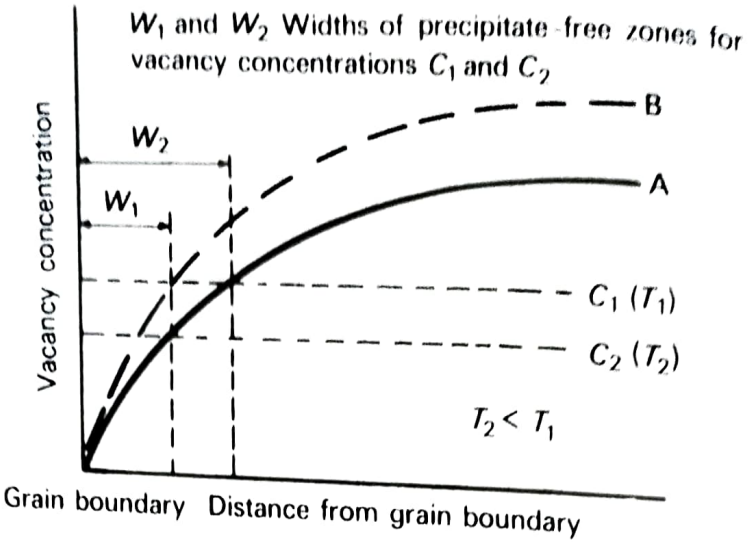

Fig. 2.8 Representation of profiles of vacancy concentration adjacent to a grain boundary in quenched alloys (from Taylor, J. L., *J. Inst. Metals*, **92**, 301, 1963–64)

2. Raising the GP zones solvus which alters the temperature ranges over which phases are stable.
3. Stimulating nucleation of an existing precipitate by reducing the interfacial energy between precipitate and matrix.
4. Promoting formation of a different precipitate.
5. Providing heterogeneous sites at which existing or new precipitates may nucleate. These sites may be clusters of atoms or actual small particles.
6. Increasing supersaturation so that the precipitation process is stimulated.

An early example of a trace element effect was the role of minor additions of cadmium, indium or tin in changing the response of binary Al–Cu alloys to age-hardening. These elements reduce room temperature (natural) ageing because they react preferentially with vacancies and thereby retard GP zone formation (mechanism 1). On the other hand, both the rate and extent of hardening at elevated temperatures (artificial ageing) are enhanced (Fig. 2.9) because these trace elements promote precipitation of a finer and more uniform dispersion of the semi-coherent phase θ′ (Al_2Cu) in preference to coherent θ″ (Table 2.2). It was first proposed that these elements are absorbed at the θ′/matrix interfaces, thereby lowering the interfacial energy required to nucleate θ′ (mechanism 3). However, as shown in Fig. 2.10, recent observations have indicated that θ′ appears to be associated with small tin clusters or particles around 5 nm in diameter which suggests that heterogeneous nucleation has occurred at the sites (mechanism 5).

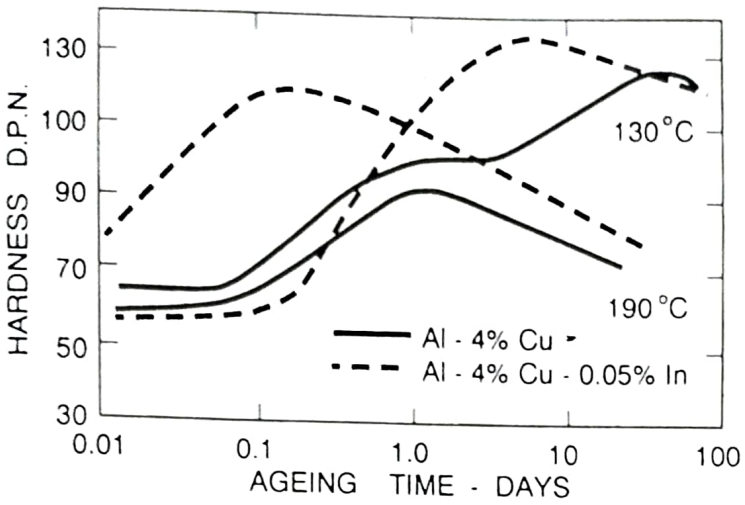

Fig. 2.9 Hardness–time curves for Al–4Cu and Al–4Cu–0.05In aged at 130 and 190°C (after Hardy, H. K., *J. Inst. Metals*,**78**, 169, 1950–51)

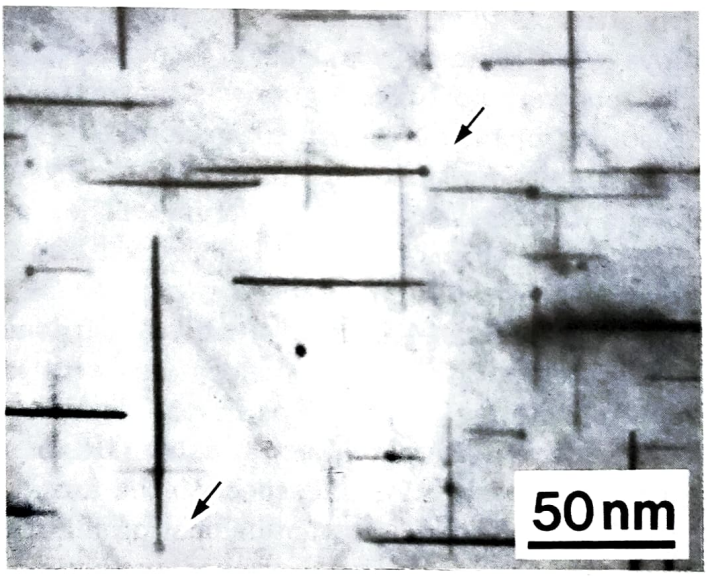

Fig. 2.10 Transmission electron micrograph showing θ′ precipitates associated with small particles of tin (courtesy S. P. Ringer, K. Hono and T. Sakurai)

Another example of a trace element effect is the role of small amounts of silver in modifying precipitation and promoting greater hardening in aluminium alloys that contain magnesium. Each system behaves differently. With Al–Zn–Mg alloys aged at elevated temperatures (e.g. Fig 2.7b), silver stimulates the existing ageing process and this effect is attributed to an increase in the temperature range over which GP zones are stable (mechanism 2). In binary Al–Mg alloys, silver may induce precipitation in alloys in which normally it is absent (mechanism 6). Of particular interest is the Al–Cu–Mg system in

which silver promotes formation of a series of new precipitates (e.g. Fig 3.18) the nature of which depends on the Cu:Mg ratio. In this case, the effects are considered to originate from clustering resulting from a preferred interaction between silver atoms, magnesium atoms and vacancies during quenching from the solution treatment temperature, or immediately after artificial ageing has commenced.

Because extensive studies above have already been made of the effects of major additions on the response of aluminium alloys to age-hardening, it is to be expected that the role of minor or trace elements will receive increasing attention. As indicated above, these elements can have important practical effects in changing microstructures and properties, some of which are discussed when considering individual alloys systems.

2.1.5 Hardening mechanisms

Although early attempts to explain the hardening mechanisms in age-hardened alloys were limited by a lack of experimental data, two important concepts were postulated. One was that hardening, or the increased resistance of an alloy to deformation, was the result of interference to slip by particles precipitating on crystallographic planes. The other was that maximum hardening was associated with a critical particle size. Modern concepts of precipitation-hardening are essentially the consideration of these two ideas in relation to dislocation theory, since the strength of an age-hardened alloy is controlled by the interaction of moving dislocations with precipitates.

Obstacles to the motion of dislocations in age-hardened alloys are the internal strains around precipitates, notably GP zones, and the actual precipitates themselves. With respect to the former, it can be shown that maximum impedence to the dislocation motion, i.e. maximum hardening, is to be expected when the spacing between particles is equal to the limiting radius of curvature of moving dislocation lines, i.e. about 50 atomic spacings or 10 nm. At this stage the dominant precipitate in most alloys is coherent GP zones, and high-resolution transmission electron microscopy has revealed that these zones are, in fact, sheared by moving dislocations. Thus individual GP zones *per se* have only a small effect in impeding glide dislocations and the large increase in yield strength these zones may cause arises because of their high volume fraction.

Shearing of the zones increases the number of solute–solvent bonds across the slip planes in the manner depicted in Fig. 2.11 so that the process of clustering tends to be reversed. Additional work must be done by the applied stress in order for this to occur, the magnitude of which is controlled by factors such as relative atomic sizes of the

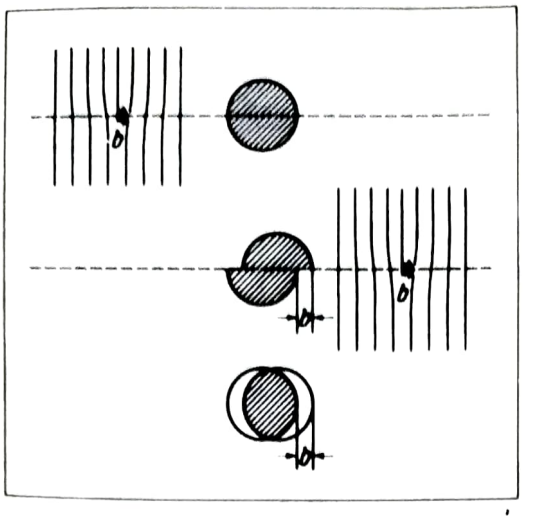

Fig. 2.11 Representation of the cutting of a fine particle, e.g. GP zone, by a moving dislocation (from Conserva, M. *et al.*, *Alumino E. Nuova Metallurgia*, **39**, 515, 1970)

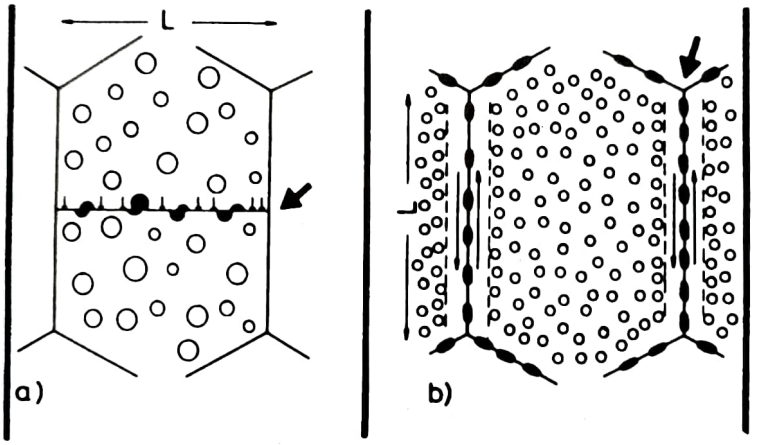

Fig. 2.12 (a) Shearing of fine precipitates leading to planar slip and dislocation pile-ups at grain boundaries; (b) Stress concentration at grain boundary triple points due to presence of precipitate-free zones (from Lütjering, G. and Gysler, A., *Aluminium Transformation, Technology and Applications*, American Society for Metals, Cleveland, Ohio, 171, 1980)

atoms concerned and the difference in stacking-fault energy between matrix and precipitate. This so-called chemical hardening makes an additional contribution to the overall strengthening of the alloy.

Once GP zones are cut, dislocations continue to pass through the particles on the active slip planes and work-hardening is comparatively small. Deformation tends to become localized on only a few active slip planes so that some intense bands develop which allows dislocations to pile up at grain boundaries in the manner shown schematically in Fig. 2.12a. As will be discussed in Sections 2.4 and 3.5.6, the development of this type of microstructure may be

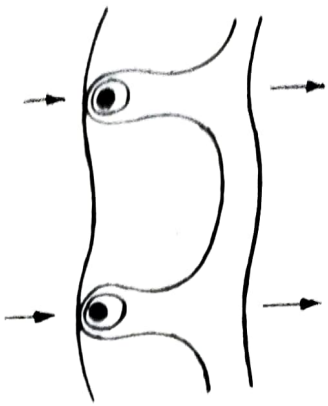

Fig. 2.13 Representation of a dislocation bypassing widely spaced particles

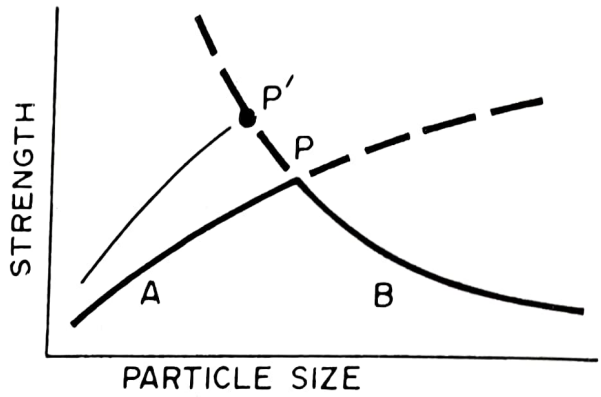

Fig. 2.14 Representation of relationship between strength and particle size for a typical age-hardening alloy: (A) particles sheared by dislocations; (B) particles not sheared (i.e. bypassed) by dislocations (from Nicholson R. B., *Strengthening Methods in Crystals*, Kelly, A. and Nicholson, R. B., Eds, Elsevier, Amsterdam, p. 535, 1971)

deleterious with respect to mechanical properties such as ductility, toughness, fatigue and stress corrosion.

If precipitate particles are large and widely spaced, they can be readily bypassed by moving dislocations which bow out between them and rejoin by a mechanism first proposed by Orowan (Fig. 2.13). Loops of dislocations are left around the particles. The yield strength of the alloy is low but the rate of work-hardening is high, and plastic deformation tends to be spread more uniformly throughout the grains. This is the situation with over-aged alloys and the typical age-hardening curve in which strength increases then decreases with ageing time has been associated with a transition from shearing (curve A) to bypassing (curve B) of precipitates, as shown schematically in Fig. 2.14. In theory, the intersection point at P represents the maximum strength that can be developed in the alloy.

Accompanying the formation of the intermediate precipitate is the development of wider, precipitate-free zones adjacent to grain boundaries as shown in Fig. 2.7(a). These zones are relatively weak with respect to the age-hardened matrix and may deform preferentially leading to high stress concentrations at triple points (Fig. 2.12b) which, in turn, may cause premature cracking (Section 2.4).

The most interesting situation arises if precipitates are present which can resist shearing by dislocations and yet be too closely spaced to allow bypassing by dislocations. In such a case, the motion of dislocation lines would only be possible if sections can pass over or under individual particles by a process such as cross-slip. High levels of both strengthening and work-hardening would then be expected. Normally such precipitates are too widely spaced for this to occur. However, some success has been achieved through the following strategies in stimulating formation of dispersions of precipitates that resist cutting by dislocations:

1. Duplex ageing treatments first below, and then above the GP zones solvus temperature which enable finer dispersions of intermediate precipitates to be formed in some alloys (e.g. Section 3.5.5).
2. Co-precipitation of two phases, one which forms as finely dispersed zones or particles that contribute mainly to raising yield strength and the other as larger particles that resist shearing by dislocations so that plastic deformation is distributed more uniformly.
3. Co-precipitation of two or more intermediate phases, each of which forms on different crystallographic planes so that dislocation mobility is again reduced (Section 3.5.6).
4. Nucleation of uniform dispersions of intermediate precipitates by the addition of specific trace elements (e.g. Fig. 3.18).

An increase in the volume fraction of precipitate particles raises both curves A and B in Fig. 2.14 resulting in higher strength. Similarly, a decrease in the particle size of precipitates that are still capable of resisting shearing by dislocations will also raise the peak strength by moving P to P′. The critical size, D_c, of particles capable of resisting shearing varies with different precipitate phases and depends on crystal structure and morphology. For example, the T_1 phase (Al_2CuLi) that forms on the $\{111\}_\alpha$ planes in certain artificially aged, lithium-containing alloys has a smaller value of D_c than the phase θ′ (Al_2Cu) that forms on the $\{100\}_\alpha$ planes (Table 2.2).

The ability of a much coarser but uniform dispersion of this T_1 phase to promote significantly greater hardening than a much higher density of zones of the fine, shearable phase θ″ in the same Al–Cu–Li–Mg–Ag–Zr alloy is illustrated in Fig. 2.15. It may also be noted that yield stresses exceeding 700 MPa have been recorded for this alloy

Table 2.2 Probable precipitation processes in aluminium alloys of commercial interest

Alloy	Precipitates	Remarks
Al–Cu	GP zones as thin plates on $\{100\}_\alpha$	Probably single layers of copper atoms on $\{100\}_\alpha$
	θ'' (formerly GP zones [2])	Coherent, probably two layers of copper atoms separated by three layers of aluminium atoms. May be nucleated at GP zones
	θ' tetragonal Al_2Cu $a = 0.404$ nm $c = 0.580$ nm	Semi-coherent plates nucleated at dislocations Form on $\{100\}_\alpha$
	θ body-centred tetragonal Al_2Cu $a = 0.607$ nm $c = 0.487$ nm	Incoherent equilibrium phase May nucleate at surface of θ'
Al–Mg (> 5%)	Spherical GP zones	GP zones solvus below room temperature if <5%Mg and close to room temperature in compositions between 5 and 10%Mg
	β' hexagonal $a = 1.002$ nm $c = 1.636$ nm	Probably semi-coherent Nucleated on dislocations $(0001)_\beta // (001)_\alpha; [01\bar{1}0]_\beta // [110]_\alpha$
	β face-centred cubic Mg_5Al_8 (formerly Mg_2Al_3) $a = 2.824$ nm	Incoherent, equilibrium phase. Forms as plates or laths in grain boundaries and at a surface of β' particles in matrix $(111)_\beta // (001)_\alpha; [110]_\beta // [010]_\alpha$
Al–Si	Silicon diamond cubic $a = 0.542$ nm	Silicon forms directly from SSSS
Al–Cu–Mg	GP (Cu, Mg) zones as rods along $<100>_\alpha$	GP zones form very rapidly in most compositions aged at elevated temperatures. Sometimes known as GPB zones
	S' orthorhombic Al_2CuMg $a = 0.404$ nm $b = 0.925$ nm $c = 0.718$ nm	Semi-choherent and nucleated at dislocations Forms as laths in $\{210\}_\alpha$ along $<001>_\alpha$

Table 2.2 *Continued*

	S orthorhomic Al_2CuMg a = 0.400 nm b = 0.923 nm c = 0.714 nm	Incoherent equilibrium phase, probably transforms from S′. Note that precipitates from the Al–Cu system can also form in compositions with high Cu:Mg ratios
Al–Mg–Si	Clusters of Mg and Si atoms. GP zones?	GP zones solvus occurs at temperatures that are normally higher than the ageing temperatures.
	β″ monoclinic a = 1.534 nm b = 0.405 nm c = 0.683 nm β = 106°	Coherent needles, lie along $\langle 100 \rangle_\alpha$ $(010)_{\beta''}$// $(001)_\alpha$; $[001]_{\beta''}$//$[310]_\alpha$
	β′ hexagonal Mg_2Si a = 0.705 nm c = 0.405 nm	Semi-coherent rods, lie along $\langle 100 \rangle_\alpha$. $(001)_{\beta'}$// $(100)_\alpha$; $[100]_{\beta'}$//$[011]_\alpha$ May form from β″?
	B′ hexagonal a = 1.04 nm c = 0.405 nm	Semi-coherent laths, lie along $\langle 100 \rangle_\alpha$. $(0001)_{B'}$//$(001)_\alpha$; $(10\bar{1}0)_{B'}$//$[510]_\alpha$ Forms together with β′; favoured by high Si:Mg ratios.
	β face-centred cubic Mg_2Si a = 0.639 nm	Platelets on $\{100\}_\alpha$. May transform directly from β′ $(100)_\beta$//$(100)_\alpha$; $[110]_\beta$//$[100]_\alpha$
Al–Zn–Mg	GP zones as spheres	Possibility of two types of zones
	η′ (or M′) hexagonal $MgZn_2$ a = 0.496 nm c = 0.868 nm	May form from GP zones in alloys with Zn:Mg > 3:1 $(0001)_{\eta'}$//$(111)_\alpha$; $[11\bar{2}0]_{\eta'}$//$[112]_\alpha$
	η (or M) hexagonal $MgZn_2$ a = 0.521 nm c = 0.860 nm	Forms at or from η′, may have one of nine orientation relationships with matrix. Most common are: $(10\bar{1}0)_\eta$//$(001)_\alpha$; $(0001)_\eta$//$(110)_\alpha$ and $(0001)_\eta$//$(1\bar{1}\bar{1})_\alpha$;$(10\bar{1}0)_\eta$//$(110)_\alpha$

Table 2.2 *Continued*

Alloy	Precipitates	Remarks
	T′ hexagonal, probably $Mg_{32}(Al, Zn)_{49}$ $a = 1.388$ nm $c = 2.752$ nm	Semi-coherent. May form instead of η in alloys with high Mg:Zn ratios $(0001)_{T'}//(111)_{\alpha}; (10\bar{1}1)_{T'}//(11\bar{2})_{\alpha}$
	T cubic $Mg_{32}(Al, Zn)_{49}$ $a = 1.416$ nm	May form from η if ageing temperature > 190°C, or from *T′* in alloys with high Mg:Zn ratios $(100)_{T}//(112)_{\alpha}$; $[001]_{T}//[100]_{\alpha}$
Al–Li–Mg	δ′ cubic Al_3Li $a = 0.404$ to 0.401 nm	Metastable coherent precipitate with ordered $Cu_3Au(Ll_2)$ type superlattice. Low misfit
	Al_2LiMg cubic $a = 1.99$ nm	Forms as coarse rods with ⟨110⟩ growth directions in alloys with >2%Mg. $(\bar{1}10)_{ppt}//(\bar{1}10)_{Al}; [110]_{ppt}//[111]_{Al}$
Al–Li–Cu	δ′ cubic Al_3Li	As for Al–Li and Al–Li–Mg alloys
	δ cubic AlLi $a = 0.637$ nm	Nucleates heterogenously, mainly in grain boundaries. $(100)_{\delta}//(100)_{\alpha}; (011)_{\delta}//(\bar{1}11)_{\alpha}; (0\bar{1}1)_{\delta}//(1\bar{1}2)_{\alpha}$
	T_1 hexagonal Al_2LiCu $a = 0.497$ nm $c = 0.934$ nm	Thin hexagonal shaped plates with {111} habit plane. $(001)_{T_1}//\{111\}_{\alpha}$; $\langle 10\bar{1}0\rangle_{T_1}//\langle\bar{1}10\rangle_{\alpha}$
	θ″, θ′	Phase present in binary Al–Cu alloys may also form at low Li:Cu ratios

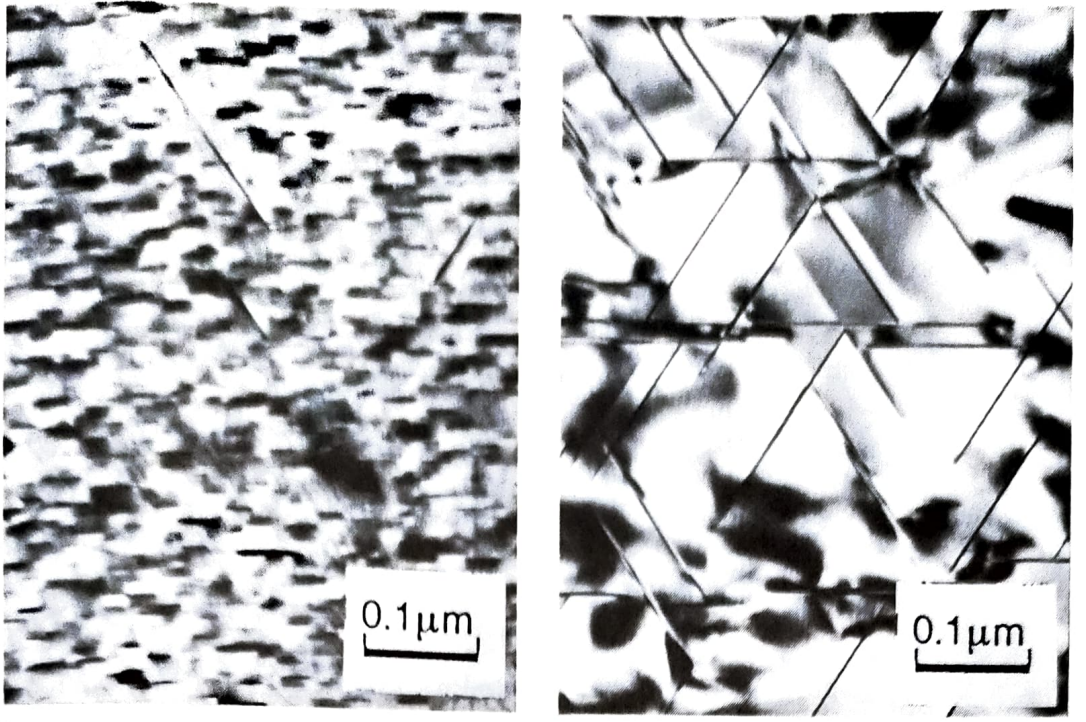

(a) (b)

Fig. 2.15 Electron micrographs of the alloy Al–5.3Cu–1.3Li–0.4Mg–0.4Ag–0.16Zr: (a) quenched and aged 8 h at 160°C showing finely dispersed, coherent θ'' particles and occasional plates of the T_1 phase. Hardness 146 DPN; (b) quenched, cold worked 6% and aged 8 h 160°C showing a much coarser but uniform dispersion of semi-coherent T_1 plates. Hardness 200 DPN (courtesy S. P. Ringer) $b = <110>_\alpha$

which is close to the theoretical upper limit of the yield stress for aluminium (approximately 900 MPa).

2.2 Ageing processes

As mentioned earlier, several aluminium alloys display a marked response to age-hardening. By suitable alloying and heat treatment, it is possible to increase the yield stress of high-purity aluminium by as much as 40 times. Details of the precipitation processes in alloy systems having commercial significance are shown in Table 2.2.

A partial phase diagram for the Al–Cu system is shown in Fig. 2.1 and the Al–Mg–Si system is represented by a pseudo-binary Al–Mg_2Si diagram in Fig. 2.16. Sections of phase diagrams for the ternary Al–Cu–Mg and Al–Zn–Mg systems are shown in Figs. 2.17 and 2.18. Most of the commercial alloys based on either system have additional alloying elements present which modify these diagrams, e.g. the section at 460°C for Al–Zn–Mg alloys containing 1.5% copper which is shown in Fig. 2.19. This is the usual solution treatment temperature for alloys of this type and it should be noted that some quaternary compositions will not be single phase after such a treatment.

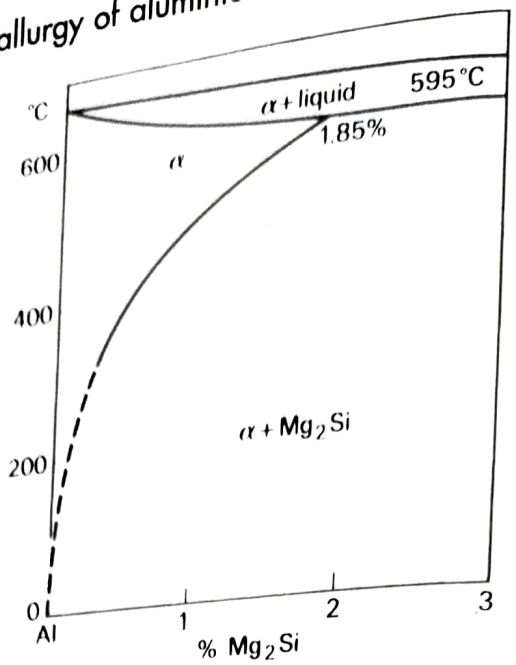

Fig. 2.16 Pseudo-binary phase diagram for Al–Mg_2Si

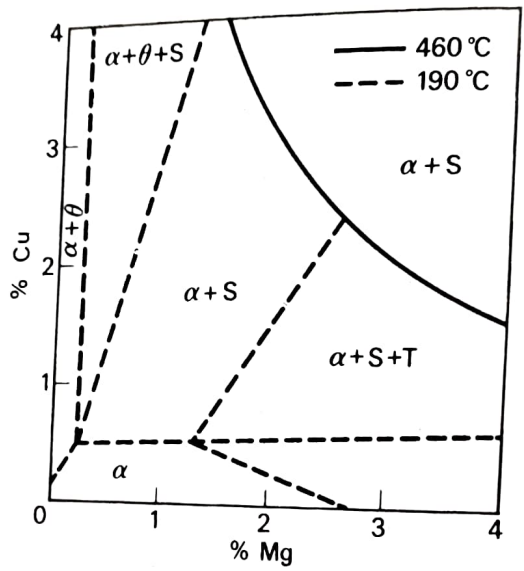

Fig. 2.17 Section of ternary Al–Cu–Mg phase diagram at 460°C and 190°C (estimated). θ = Al_2Cu, S = Al_2CuMg, T = Al_6CuMg_4

2.3 Corrosion

2.3.1 Surface oxide film

Aluminium is an active metal which will oxidize readily under the influence of the high free energy of the reaction whenever the necessary conditions for oxidation prevail. Nevertheless, aluminium and its alloys are relatively stable in most environments due to the rapid formation of a natural oxide film of alumina on the surface that

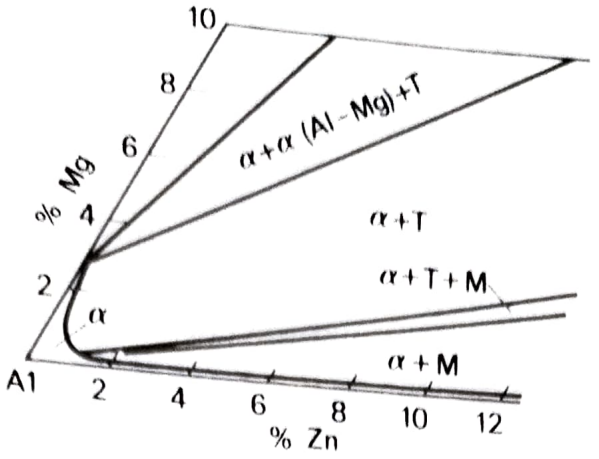

Fig. 2.18 Section of ternary Al–Zn–Mg phase diagrams at 200°C. M = $MgZn_2$, T = Al_{32} $(Mg,Zn)_{49}$

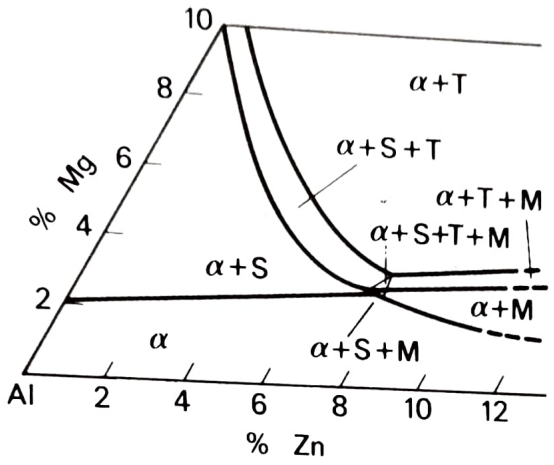

Fig. 2.19 Section of Al–Zn–Mg–Cu phase diagram (1.5% Cu) at 460°C. S = Al_2 CuMg, T = Al_6CuMg_4 + Al_{32} $(Mg,Zn)_{49}$, M = $MgZn_2$ + AlCuMg

inhibits the bulk reaction predicted from thermodynamic data. Moreover, if the surface of aluminium is scratched sufficiently to remove the oxide film, a new film quickly re-forms in most environments. As a general rule, the protective film is stable in aqueous solutions of the pH range 4.5–8.5, whereas it is soluble in strong acids or alkalis, leading to rapid attack of the aluminium. Exceptions are concentrated nitric acid, glacial acetic acid and ammonium hydroxide.

The oxide film formed on freshly rolled aluminium exposed to air is very thin and has been measured as 2.5 nm. It may continue to grow at a decreasing rate for several years to reach a thickness of some tens of nanometres. The rate of film growth becomes more rapid at higher temperatures and higher relative humidities, so in water it is many times that occurring in dry air. In aqueous solutions, it has been suggested that the initial corrosion product is aluminium hydroxide, which changes with time to become a hydrated aluminium oxide. The

main difference between this film and that formed in air is that it is less adherent and so is far less protective.

Much thicker surface oxide films that give enhanced corrosion resistance to aluminium and its alloys can be produced by various chemical and electrochemical treatments. The natural film can be thickened some 500 times, to say 1–2 μm, by immersion of components in certain hot acid or alkaline solutions. Although the films produced are mainly Al_2O_3, they also contain chemicals such as chromates which are collected from the bath to render them more corrosion resistant. A number of proprietary solutions are available and the films they produce are known generally as conversion coatings. Even thicker, e.g. 10–20 μm, surface films are produced by the more commonly used treatment known as anodizing. In this case the component is made the anode in an electrolyte, such as an aqueous solution containing 15% sulphuric acid, which produces a porous Al_2O_3 film that is subsequently sealed, i.e. rendered non-porous, by boiling in water. Both conversion and anodic coatings can be dyed to give attractive colours and the latter process is widely applied to architectural products.

It should be noted that chromate conversion coatings are widely used in corrosion protection schemes for aluminium alloys in aircraft structures and other applications. However, it has been recognized recently that chromates may present a health hazard which has led to an interest in other, non-toxic, coating processes. Promising results have been reported for cerium-rich coatings which can be applied by several methods. A durable cerium oxide/hydroxide film replaces natural Al_2O_3 and protection is afforded by partial or complete suppression of the reduction of oxygen at cathodic sites which normally occurs during electrolytic corrosion.

2.3.2 Contact with dissimilar metals

The electrode potential of aluminium with respect to other metals becomes particularly important when considering galvanic effects arising from dissimilar metal contact. Comparisons must be made by taking measurements in the same solution and Table 2.3 shows the electrode potentials with respect to the 0.1 M calomel electrode ($Hg–HgCl_2$, 0.1 M KCl) for various metals and alloys immersed in an aqueous solution of 1 M NaCl and 0.1 M H_2O_2. The value for aluminium is −0.85 V whereas aluminium alloys range from −0.69 V to −0.99 V. Magnesium which has an electrode potential of −1.73 V is more active than aluminium whereas mild steel is cathodic having a value of − 0.58 V.

Table 2.3 suggests that sacrificial attack of aluminium and its alloys

Table 2.3 Electrode potentials of various metals and alloys with respect to the 0.1 M calomel electrode in aqueous solutions of 53 g l^{-1} NaCl and 3 g l^{-1} H_2O_2 at 25°C (from *Metals Handbook*, Volume 1, American Society for Metals, Cleveland, Ohio, 1961)

Metal or alloy		Potential (V)
Magnesium		− 1.73
Zinc		− 1.10
Alclad 6061, Alclad 7075	aluminium alloys*	− 0.99
5456, 5083		− 0.87
Aluminium (99.95%), 5052, 5086		− 0.85
3004, 1060, 5050		− 0.84
1100, 3003, 6063, 6061, Alclad 2024		− 0.83
2014–T4		− 0.69
Cadmium		− 0.82
Mild steel		− 0.58
Lead		− 0.55
Tin		− 0.49
Copper		− 0.20
Stainless steel (3xx series)		− 0.09
Nickel		− 0.07
Chromium		− 0.49 to + 0.18

* Compositions corresponding to the numbers are given in Tables 3.2 and 3.4

will occur when they are in contact with most other metals in a corrosive environment. However, it should be noted that electrode potentials serve only as a guide to the possibility of galvanic corrosion. The actual magnitude of the galvanic corrosion current is determined not only by the difference in electrode potentials between the particular dissimilar metals but also by the total electrical resistance, or polarization, of the galvanic circuit. Polarization itself is influenced by the nature of the metal/liquid interface and more particularly by the oxides formed on metal surfaces. For example, contact between aluminum and stainless steels usually results in less electrolytic attack than might be expected from the relatively large difference in the electrode potentials, whereas contact with copper causes severe galvanic corrosion of aluminium even though this difference is less.

2.3.3 Influence of alloying elements and impurities

Alloying elements may be present as solid solutions with aluminium, or as micro-constituents comprising the element itself, e.g. silicon, a compound between one or more elements and aluminium (e.g. Al_2CuMg) or as a compound between one or more elements (e.g. Mg_2Si). Any or all of the above conditions may exist in a commercial

Table 2.4 Electrode potentials of aluminum solid solutions and micro-constituents with respect to the 0.1 M calomel electrode in aqueous solutions of 53 g l^{-1} NaCl and 3 g l^{-1} H_2O_2 at 25°C (from *Metals Handbook, Volume 1, American Society for Metals, Cleveland, Ohio, 1961)*

Solid solution or micro-constituent	Potential (V)
Mg_5Al_8	− 1.24
Al–Zn–Mg solid solution (4% $MgZn_2$)	− 1.07
$MgZn_2$	− 1.05
Al_2CuMg	− 1.00
Al–5% Mg solid solution	− 0.88
$MnAl_6$	− 0.85
Aluminium (99.95%)	− 0.85
Al–Mg–Si solid solution (1% Mg_2Si)	− 0.83
Al–1% Si solid solution	− 0.81
Al–2% Cu supersaturated solid solution	− 0.75
Al–4% Cu supersaturated solid solution	− 0.69
$FeAl_3$	− 0.56
$CuAl_2$	− 0.53
$NiAl_3$	− 0.52
Si	− 0.26

alloy. Table 2.4 gives values of the electrode potentials of some aluminium solid solutions and micro-constituents.

In general, a solid solution is the most corrosion resistant form in which an alloy may exist. Magnesium dissolved in aluminium renders it more anodic although dilute Al–Mg alloys retain a relatively high resistance to corrosion, particularly to sea water and alkaline solutions. Chromium, silicon and zinc in solid solution in aluminium have only minor effects on corrosion resistance although zinc does cause a significant increase in the electrode potential. As a result, Al–Zn alloys are used as clad coatings for certain aluminium alloys (see Section 3.1.5) and as galvanic anodes for the cathodic protection of steel structures in sea water. Copper reduces the corrosion resistance of aluminium more than any other alloying element and this arises mainly because of its presence in micro-constituents. However, it should be noted that when added in small amounts (0.05–0.2%), corrosion of aluminium and its alloys tends to become more general and pitting attack is reduced. Thus, although under corrosive conditons the overall weight loss is greater, perforation by pitting is retarded.

Micro-constituents are usually the source of most problems with electrochemical corrosion as they lead to non-uniform attack at specific areas of the alloy surface. Pitting and intergranular corrosion are examples of localized attack (Fig. 2.20), and an extreme example of this is that components with a marked directionality of

Fig. 2.20 Microsection of surface pits in a high-strength aluminium alloy. Note that intergranular stess-corrosion cracks are propagating from the base of these pits (× 100)

Fig. 2.21 Microsection showing exfoliation (layer) corrosion of an aluminium alloy plate (× 100)

grain structure show exfoliation (layer) corrosion (Fig. 2.21). In exfoliation corrosion, delamination of surface grains or layers occurs under forces exerted by the voluminous corrosion products.

Iron and silicon occur as impurities and form compounds most of which are cathodic with respect to aluminium. For example, the compound Al_3Fe provides points at which the surface oxide film is weak, thereby promoting electrochemical attack. The rate of general

corrosion of high-purity aluminium is much less than that of the commercial-purity grades which is attributed to the smaller size and number of these cathodic constituents throughout the grains. However, it should be noted that this may be a disadvantage in some environments as attack of high-purity aluminium may be concentrated in grain boundaries. Nickel and titanium also form cathodic phases although nickel is present in very few alloys. Titanium, which forms Al_3Ti, is commonly added to refine grain size (Section 3.1.3) but the amount is too small to have a significant effect on corrosion resistance. Manganese and aluminium form Al_6Mn, which has almost the same electrode potential as aluminium, and this compound is capable of dissolving iron which reduces the detrimental effect of this element. Magnesium in excess of that in solid solution in binary aluminium alloys tends to form the strongly anodic phase Mg_5Al_8 which precipitates in grain boundaries and promotes intercrystalline attack. However, magnesium and silicon, when together in the atomic ratio 2:1, form the phase Mg_2Si which has a similar electrode potential to aluminium.

2.3.4 Metallurgical and thermal treatments

Treatments that are carried out to change the shape and achieve a desired level of mechanical properties in aluminium alloys may also modify corrosion resistance, largely through their effects on both the quantity and the distribution of micro-constituents. In this regard, the complex changes associated with ageing or tempering treatments are on a fine scale and these are considered in Chapter 3. Both mechanical and thermal treatments can introduce residual stresses into components which may contribute to the phenomenon of stress-corrosion cracking and this is discussed in Section 2.4.4.

If one portion of an alloy surface receives a thermal treatment different from the remainder of the alloy, differences in potential between these regions can result. Welding processes provide an extreme example of such an effect and differences of up to 0.1 V may exist between the weld bead, heat-affected zones and the remainder of the parent alloy.

Most wrought products do not undergo bulk recrystallization during subsequent heat treatment so that the elongated grain structure resulting from mechanical working is retained. Three principal directions are recognized: longitudinal, transverse (or long transverse) and short transverse, and these are represented in Fig. 2.22. This directionality of grain structure is significant in components when corrosion processes involve intercrystalline attack as has been illustrated

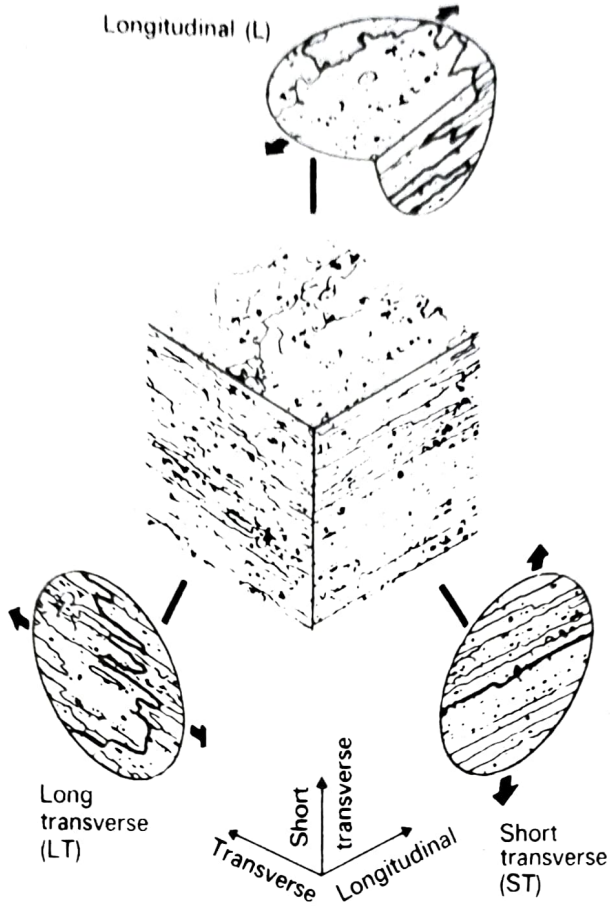

Fig. 2.22 The three principal directions with respect to the grain structure in a wrought aluminium alloy. Note the appearance of cracks that may form when stressing in these three directions (from Speidel, M. O. and Hyatt, M. V., *Advances in Corrosion Science and Technology*, Plenum Press, New York, 1972)

by exfoliation corrosion. It is particularly important in regard to stress–corrosion cracking, which is discussed in Section 2.4.4.

In certain products such as extrusions and die forgings, working is non-uniform and a mixture of unrecrystallized and recrystallized grain structures may form between which potential differences may exist. Large, recrystallized grains normally occur at the surface (see Fig. 3.7) and these are usually slightly cathodic with respect to the underlying, unrecrystallized grains. Preferential attack may occur if the relatively more anodic internal grains are partly exposed as may occur by machining.

2.4 Mechanical behaviour

The principal microstructural features that control the mechanical properties of aluminium alloys are as follows:

1. Coarse intermetallic compounds (often called constituent particles) that form interdendritically by eutectic decomposition during ingot solidification. One group comprises virtually insoluble compounds that usually contain the impurity elements iron or silicon and examples are $Al_6(Fe,Mn)$, Al_3Fe, $\alpha Al(Fe,Mn,Si)$ and Al_7Cu_2Fe. The second group, which are known as the soluble constituents, consists of equilibrium intermetallic compounds of the major alloying elements. Typical examples are Al_2Cu, Al_2CuMg, and Mg_2Si. Both types of particles form as lacy networks surrounding the cast grains and one purpose of the process referred to as preheating or ingot homogenization (Section 3.1.4) is to dissolve the soluble constituents. During subsequent fabrication of the cast ingots, the largest of the remaining particles usually fracture, which reduces their sizes to the range 0.5–10 μm and causes them to become aligned as stringers in the direction of working or metal flow (Fig. 2.23).

   Constituent particles serve no useful function in high-strength wrought alloys and they are tolerated in most commercial compositions because their removal would necessitate a significant cost increase. They do, however, serve a useful purpose in certain alloys such as those used for canstock (Section 3.7.3).
2. Smaller submicron particles, or dispersoids (typically 0.05–0.5 μm)

Fig. 2.23 Aligned stringers of coarse intermetallic compounds in a rolled aluminium alloy (× 250)

that form during homogenization of the ingots by solid state precipitation of compounds containing elements which have modest solubility and which diffuse slowly in solid aluminium. Once formed, these particles resist either dissolution or coarsening. The compounds usually contain one of the transition metals and examples are $Al_{20}Mn_3Cu_2$, $Al_{12}Mg_2Cr$ and Al_3Zr. They serve to retard recrystallization and grain growth during processing and heat treatment of the alloys concerned. Moreover, they may also exert an important influence on certain mechanical properties through their effects both on the response of some alloys to ageing treatments, and on dislocation substructures formed as a result of plastic deformation.

3. Fine precipitates (up to 0.1 μm) which form during age-hardening and normally have by far the largest effect on strengthening of alloys that respond to such treatments.
4. Grain size and shape. The most significant microstructural feature that differentiates wrought products such as sheet from plate, forgings and extrusions is the degree of recrystallization. Aluminium dynamically recovers during hot deformation producing a network of subgrains and this characteristic is attributed to its relatively high stacking-fault energy. However, thick sections, which experience less deformation, usually do not undergo bulk recrystallization during processing so that an elongated grain structure is retained (Fig. 2.22).
5. Dislocation substructure, notably that caused by cold working of those alloys which do not respond to age-hardening, and that developed due to service stresses.
6. Crystallographic textures that form as a result of working and annealing, particularly in rolled products. They have a marked effect on formability (Section 3.3.3) and lead to anisotropic mechanical properties.

Each of these features may be influenced by the various stages involved in the solidification and processing of wrought and cast alloys and these are discussed in detail in Chapters 3 and 4. Here it is relevant to consider how these features influence mechanical behaviour.

2.4.1 Tensile properties

Aluminium alloys may be divided into two groups depending upon whether or not they respond to precipitation hardening. The tensile properties of commercial wrought and cast compositions are considered in Chapters 3 and 4 respectively. For alloys that do respond to

ageing treatments, it is the finely dispersed precipitates that have the dominant effect in raising yield and tensile strengths. For the other group, the dislocation substructure produced by cold-working in the case of wrought alloys and the grain size of cast alloys are of prime importance.

Coarse intermetallic compounds have relatively little effect on yield or tensile strength but they can cause a marked loss of ductility in both the cast and wrought products. The particles may crack at small plastic strains forming internal voids which, under the action of further plastic strain, may coalesce leading to premature fracture.

As mentioned above, the fabrication of wrought products may cause highly directional grain structures. Moreover, the coarse intermetallic compounds and smaller dispersoids also become aligned to form stringers in the direction of metal flow (Fig. 2.23). These microstructural features are known as mechanical fibring and, together with crystallographic texturing (Section 3.3.3), they cause anisotropy in tensile and other properties. Accordingly, measurements are often made in the three principal directions shown in Fig. 2.22. Tensile properties, notably ductility, are greatest in the longitudinal direction and least in the short transverse direction in which stressing is normal to the stringers of intermetallics, e.g. Table 2.5.

2.4.2 Toughness

Early work on the higher strength aluminium alloys was directed primarily at maximizing tensile properties in materials for aircraft

Table 2.5 Variation in tensile properties with direction in 76 mm thick aluminium alloy plates (from Forsyth, P.J.E. and Stubbington, A., *Metals Technology*, **2**, 158, 1975)

Alloy direction	0.2% proof stress (MPa)	Tensile strength (MPa)	Elongation (%)
Al–Zn–Mg–Cu (7075)			
Longitudinal (L)	523	570	15.5
Long transverse (LT)	482	552	12.0
Short transverse (ST)	445	527	7.5
ST/L ratio	0.85	0.93	0.48
Al–Cu–Mg (2014)			
Longitudinal (L)	441	477	14.0
Long transverse (LT)	423	471	10.5
Short transverse (ST)	404	449	4.0
ST/L ratio	0.91	0.94	0.29

construction. More recently, the emphasis in alloy development has shifted away from tensile strength as an over-riding consideration and more attention is being given to the behaviour of alloys under the variety of conditions encountered in service. Tensile strength controls resistance to failure by mechanical overload but, in the presence of cracks and other flaws, it is the toughness (and more particularly the fracture toughness) of the alloy that becomes the most important parameter.

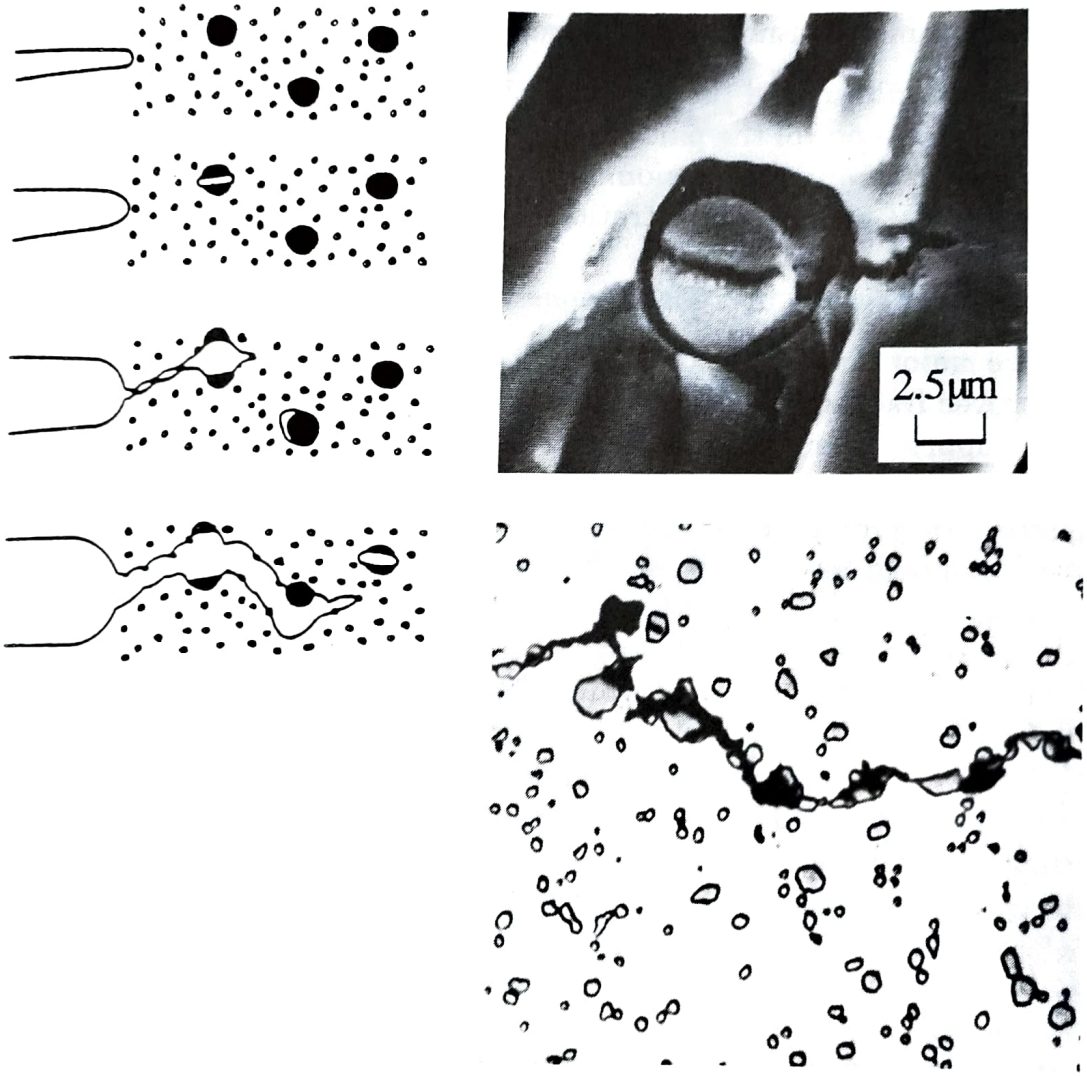

Fig. 2.24 Crack extension by coalescence of microvoids nucleated at particles and dispersoids: (a) schematic showing nucleation of voids due to particle cleavage followed by progressive linkage of advancing crack to these voids (courtesy R. J. H. Wanhill); (b) cleavage of an Al_7Cu_2Fe intermetallic particle with associated void nucleation and crack extension into the adjacent ductile matrix in a high-strength aluminium alloy. Scanning electron micrograph ×2800 (courtesy R. Gürbüz); (c) crack path in an aluminium casting alloy which has been influenced by the presence of coarse, brittle silicon particles. Optical micrograph ×700 (courtesy R.W. Coade)

In common with other metallic materials, the toughness of aluminium alloys decreases as the general level of strength is raised by alloying and heat treatment. Minimum fracture toughness requirements become more stringent and, in the high-strength alloys, it is necessary to place a ceiling on the level of yield strength that can be safely employed by the designer.

Crack extension in commercial aluminium alloys proceeds by the ductile, fibrous mode involving the growth and coalescence of voids nucleated by cracking or by decohesion at the interface between second phase particles and the matrix (Fig. 2.24). Consequently, the important metallurgical factors are:

1. The distribution of the particles that crack.
2. The resistance of the particles and their interfaces with the matrix to cleavage and decohesion.
3. The local strain concentrations which accelerate coalescence of the voids.
4. The grain size when coalescence involves grain boundaries.

The major step in the development of aluminium alloys with greatly improved fracture toughness has come from the control of the levels of the impurity elements iron and silicion. This effect is shown in Fig. 2.25 for alloys based on the Al–Cu–Mg system and it can be seen that plane strain fracture toughness values may be doubled by maintaining the combined levels of these elements below 0.5% as compared with similar alloys in which this value exceeds 1.0%. As a consequence of this, a range of high-toughness versions of older alloy compositions is now in commercial use in which the levels of impurities have been reduced (see Table 3.4).

The role of the submicron dispersoids with respect to toughness is more complex as they have both good and bad effects. To the extent that they suppress recrystallization and limit grain growth they are beneficial. The effect of these factors on a range of high-strength sheet alloys based on the Al–Zn–Mg–Cu system is shown in Fig 2.26. Fine, unrecrystallized grains favour a high energy absorbing, transcrystalline mode of fracture. On the other hand, such particles also nucleate microvoids by decohesion at the interface with the matrix which may lead to the formation of sheets of voids between the larger voids that are associated with the coarse intermetallic compounds. In this regard, the effects do vary with different transition metals and there is evidence to suggest that alloys containing zirconium to control grain shape are more resistant to fracture than those to which chromium or manganese has been added to this purpose. This is attributed to the fact that zirconium forms relatively small particles of the compound Al_3Zr, which are around 20 nm in diameter.

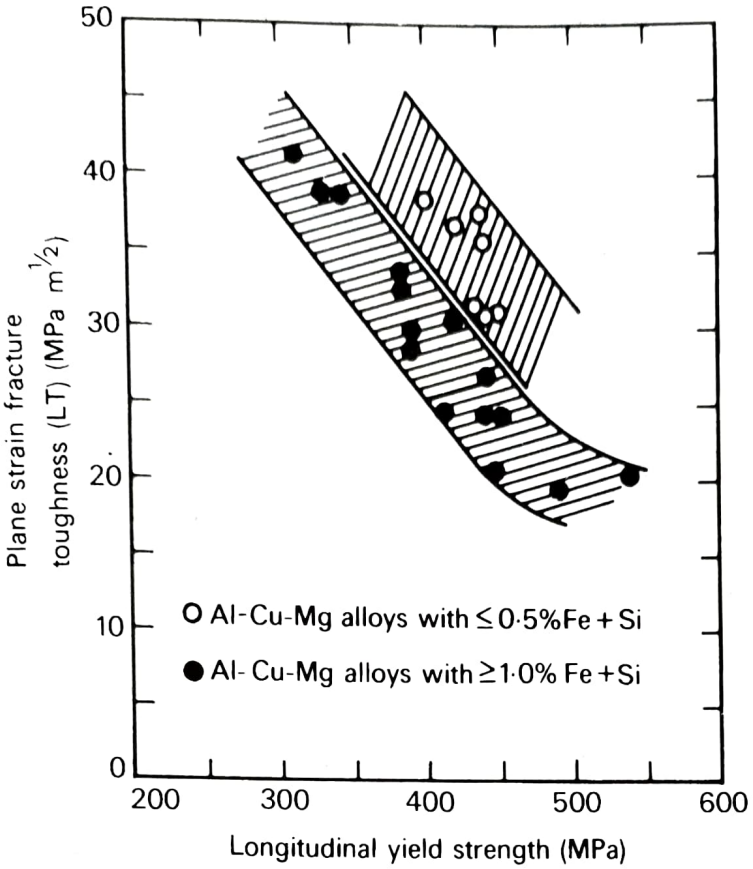

Fig. 2.25 Plane strain fracture toughness of commercial Al–Cu–Mg sheet alloys with differing levels of iron and silicon (from Speidel, M. O., *Proceedings of 6th International Conference on Light Metals*, Leoben, Austria, Aluminium-Verlag, Düsseldorf, 1975)

The fine precipitates developed by age-hardening are also thought to have at least two effects with regard to the toughness of aluminium alloys. To the extent that they reduce deformation, toughness is enhanced and it has been observed that, for equal dispersions of particles, an alloy with a higher yield stress has greater toughness. At the same time, these fine particles tend to cause localization of slip during plastic deformation, particularly under plane strain conditions, leading to development of pockets of slip or so-called superbands ahead of an advancing crack. Strain is concentrated within these bands and may cause premature cracking at the sites of intermetallic compounds ahead of an advancing crack. This effect is usually greatest for alloys aged to peak hardness and the overall result is a net loss of toughness at the highest strength levels.

The fact that toughness does not follow a simple inverse relationship to the strength of age-hardened aluminium alloys is shown by comparing alloys in the under- and over-aged conditions. Toughness is greatest in the underaged condition and decreases as ageing proceeds

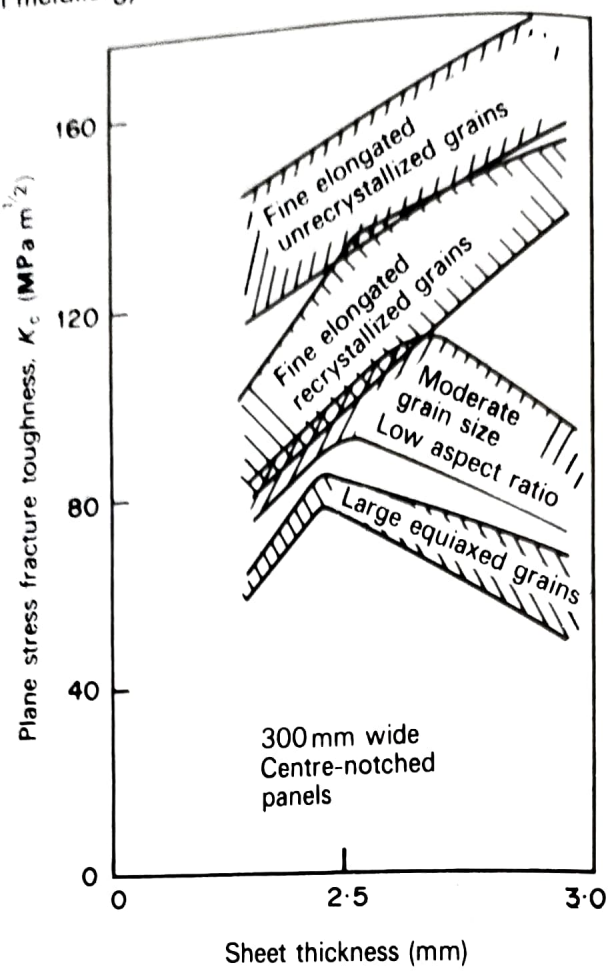

Fig. 2.26 Effect of recrystallization and grain size and shape of various alloys based on the Al–Zn–Mg–Cu system (from Thompson, D. S., *Met. Trans.*, 6A, 671, 1975)

to peak strength. In some alloys, this condition corresponds to a minimum value of toughness and some improvement may occur on over-ageing which is associated with a reduction in yield strength (e.g. Al–Zn–Mg–Cu alloys: Section 3.5.5). However, where over-ageing leads to the formation of large precipitate particles in grain boundaries, or wide precipitate-free zones then toughness can continue to decrease because each of these features promotes more intergranular fracture. Lithium-containing alloys tend to behave in this way (Section 3.5.6).

2.4.3 Fatigue

It is well known that, contrary to steels, the increases that have been achieved in the tensile strength of most non-ferrous alloys have not been accompanied by proportionate improvements in fatigue properties. This feature is illustrated in Fig. 2.27 which shows relationships between fatigue endurance limit (5×10^8 cycles) and tensile strength

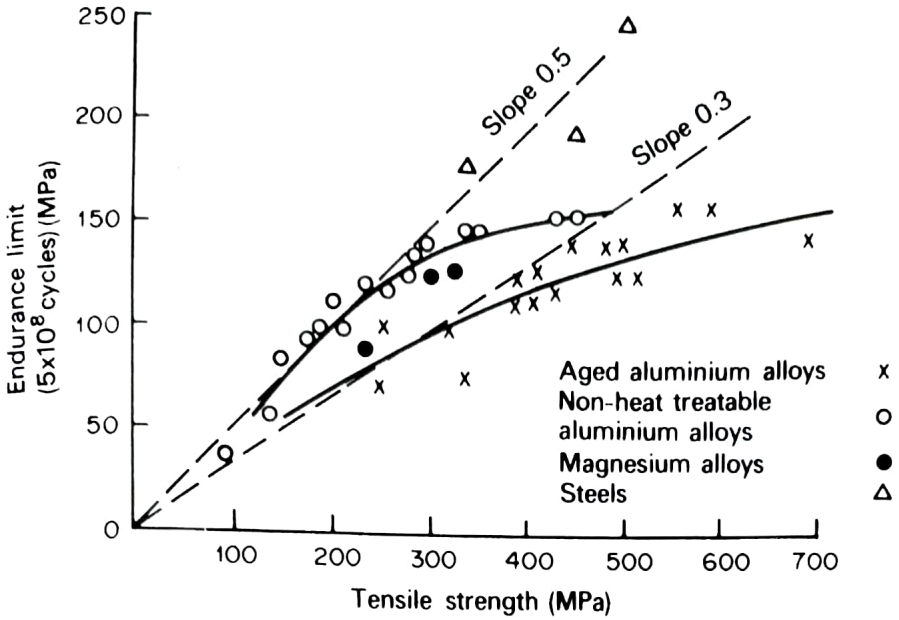

Fig. 2.27 Fatigue ratios (endurance limit: tensile strength) for aluminium alloys and other materials (from Varley, P. C., *The Technology of Aluminium and its Alloys*, Newnes-Butterworths, London, 1970)

for different alloys. It should also be noted that the so-called fatigue ratios are lowest for age-hardened aluminium alloys and, as a general rule, the more an alloy is dependent upon precipitation-hardening for its tensile strength, the lower its ratio becomes.

Detailed studies of the processes of fatigue in metals and alloys have shown that the initiation of cracks normally occurs at the surface. It is here that strain becomes localized due to the presence of pre-existing stress concentrations such as mechanical notches or corrosion pits, coarse (persistent) slip bands in which minute extrusions and intrusions may form, or at relatively soft zones such as the precipitate-free regions adjacent to grain boundaries.

The disappointing fatigue properties of age-hardened aluminium alloys are also attributed to an additional factor, and that is the metastable nature of the metallurgical structure under conditions of cyclic stressing. Localization of strain is particularly harmful because the precipitate may be removed from certain slip bands which causes softening there and leads to a further concentration of stress so that the whole process of cracking is accelerated. This effect is shown in an exaggerated manner in a recrystallized, high-purity alloy in Fig. 2.28. It has been proposed that removal of the precipitate occurs either by over-ageing or re-solution, the latter now being considered to apply in most cases. One suggestion is that the particles in the slip bands are cut by moving dislocations, and re-solution occurs

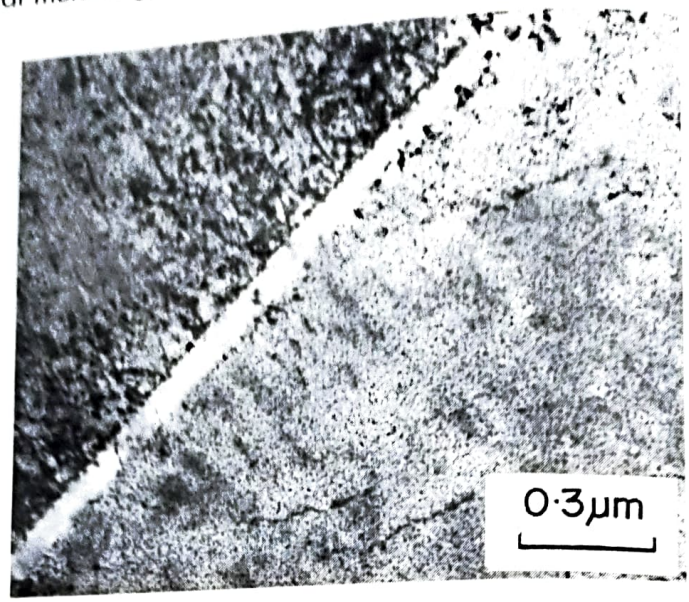

Fig. 2.28 Transmission electron micrograph showing precipitate depletion in a persistent slip band formed by fatigue stressing a high-purity Al–Zn–Mg alloy (courtesy A. Stubbington, copyright HMSO)

when they become smaller than the critical size for thermodynamic stability.

The fatigue behaviour of age-hardened aluminium alloys should therefore be improved if fatigue deformation could be dispersed more uniformly. Factors which prevent the formation of coarse slip bands should assist in this regard. Thus it is to be expected that commercial-purity alloys should perform better than equivalent high-purity compositions because the presence of inclusions and intermetallic compounds would tend to disperse slip. This effect is demonstrated for the Al–Zn–Mg–Cu alloy 7075 in Fig. 2.29 (a) which shows fatigue (S/N) curves for commercial-purity and high-purity compositions. Tests were carried out on smooth specimens prepared from the alloys which had been aged under similar conditions to produce fine, shearable precipitates. It will be noted that the fatigue performance of the commercial-purity alloys is superior because crack initiation is delayed due to the fact that slip is more uniformly dispersed by dispersoid particles such as $Al_{12}Mg_2Cr$. These particles are absent in the high-purity alloy. However, the fatigue performance characteristics are reversed if tests are carried out on pre-cracked specimens (Fig 2.29 b). In this condition, the rate of fatigue crack growth is faster in the commercial-purity alloy because voids nucleate more readily at dispersed particles which are within the plastic zone of the advancing crack (Fig. 2.24).

Thermomechanical processing whereby plastic deformation before, or during, the ageing treatment increases the dislocation density, has

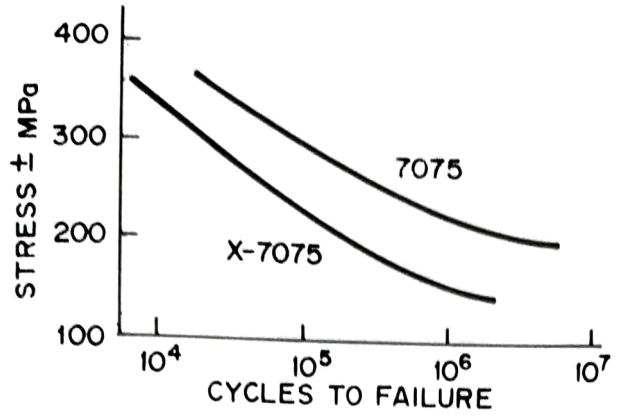

(a)

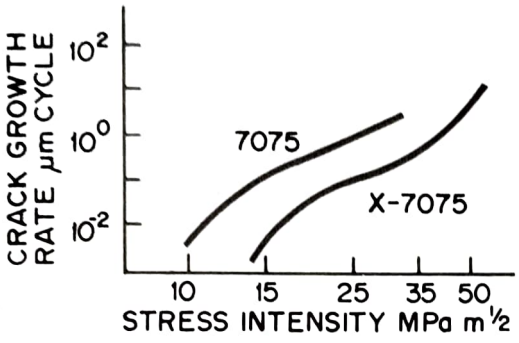

(b)

Fig. 2.29 (a) Fatigue (S/N) curves for Al–Zn–Mg–Cu alloys 7075 and X7075. X7075 is a high-purity version of the commercial alloy 7075 (from Lütjering, G., *Micromechanisms in Particle-hardened Alloys*, Martin, J. W., Cambridge University Press, 142, 1980); (b) Fatigue crack growth rate curves for alloys 7075 and X7075 (from Albrecht, J. *et al.*, *Proc. 4th Inter. Conf. on Strength of Metals and Alloys, J. de Physique*, Paris, 463, 1976)

also been found to improve the fatigue performance of certain alloys although this effect arises in part from an increase in tensile properties caused by such a treatment (Fig. 2.30). It should be noted, however, that the promising results mentioned above were obtained for smooth specimens. The improved fatigue behaviour has not been sustained for severely notched conditions and it seems that the resultant stress concentrations over-ride the more subtle microstructural effects that have been described.

Alloys which are aged at higher temperatures, and thus form relatively more stable precipitates, might also be expected to show better fatigue properties and this trend is observed. For example, the fatigue performance of the alloys based on the Al–Cu–Mg system is generally better than that of Al–Zn–Mg–Cu alloys, although this effect is again greatly reduced for notched conditions.

The fact that the microstructure can have a greater influence upon the fatigue properties of aluminium alloys than the level of tensile properties has been demonstrated for an Al–Mg alloy containing a

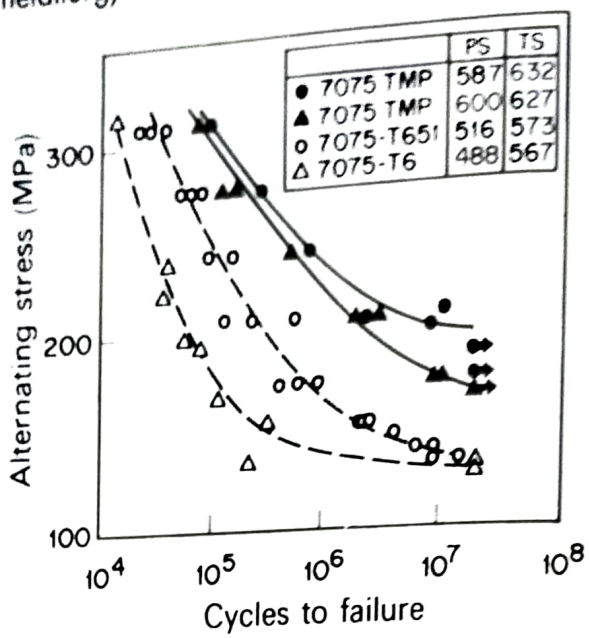

Fig. 2.30 Effect of thermomechanical processing (TMP) on the unnotched fatigue properties of the commercial Al–Zn–Mg–Cu alloy 7075. PS = proof stress (MPa), TS = tensile strength (MPa) (from Ostermann, F. G., *Met. Trans.*, **2A**, 2897, 1971)

small addition of silver. It is well known that binary Al–Mg alloys such as Al–5Mg, in which the magnesium is present in solid solution, display a relatively high level of fatigue strength. The same applies for an Al–5Mg–0.5Ag alloy in the as-quenched condition and Fig. 2.31 shows that the endurance limit after 10^8 cycles is ± 87 MPa which approximately equals the 0.2% proof stress. This result is attributed to the interaction of magnesium atoms with dislocations which minimizes formation of coarse slip bands during fatigue. The silver-containing alloy responds to age-hardening at elevated temperatures due to the formation of a finely dispersed precipitate, and the 0.2% proof stress may be raised to 200 MPa after ageing for one day at 175°C. However, the endurance limit for 10^8 cycles is actually decreased to ± 48 MPa due to the localization of strain in a limited number of coarse slip bands (Fig. 2.32a).

Continued ageing of the alloy at 175°C causes only slight softening (0.2% proof stress 175 MPa after 70 days) although large particles of a second precipitate are formed (Fig. 2.32b) which have the effect of dispersing dislocations generated by cyclic stressing. As a result, fatigue properties are improved and the endurance limit for 10^8 cycles is raised to ± 72 MPa (Fig. 2.31). These particles serve the same role as the submicron particles in the commercial alloy 7075 (Fig. 2.29) but they have formed by a precipitation process. This again suggests the desirability of having a duplex precipitate structure; fine particles to give a high level of tensile properties, and coarse particles to improve fatigue strength.

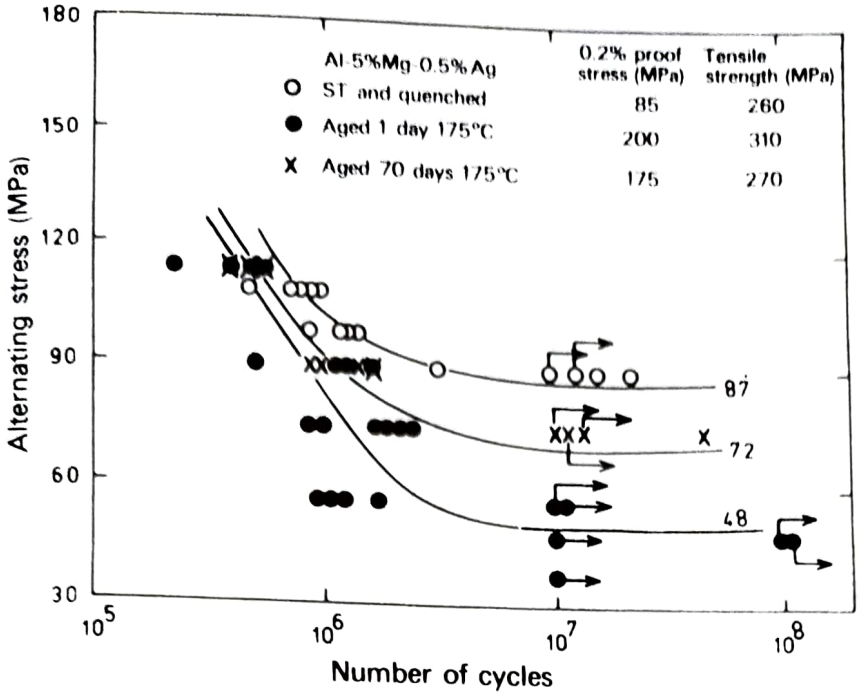

Fig. 2.31 Fatigue (S/N) curves for the alloy Al–5Mg–0.5Ag in different conditions (from Boyapati, K. and Polmear, I. J., *Fatigue of Engineering Materials and Structures*, **2**, 23, 1979)

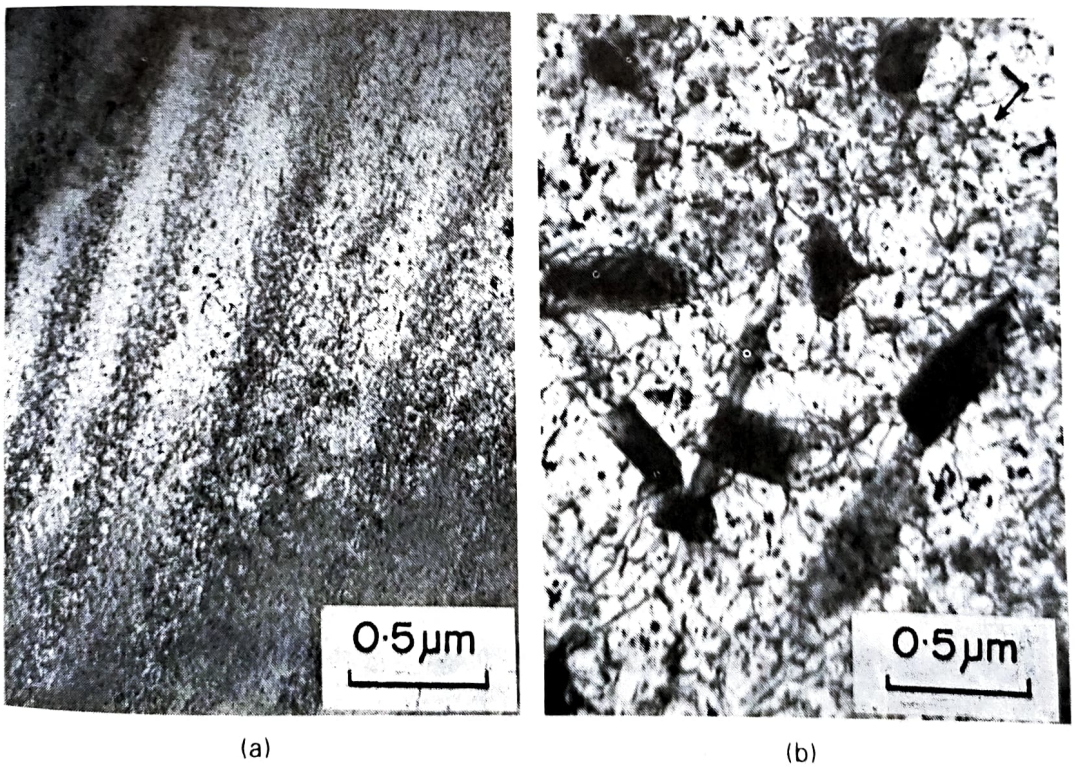

Fig. 2.32 (a) Coarse slip bands containing a high density of dislocations. Alloy Al–5Mg–0.5Ag aged one day at 175°C and tested at a stress of ± 75 MPa for 1.4×10^6 cycles; (b) large particles of a second precipitate, that have formed in the alloy aged 70 days at 175°C, which have dispersed dislocations (see arrow) generated by fatigue stressing for 10^7 cycles at a stress of ± 75 MPa

2.4.4 Stress-corrosion cracking

Stress-corrosion cracking (SCC) may be defined as a phenomenon which results in brittle failure in alloys, normally considered ductile, when they are exposed to the simultaneous action of surface tensile stress and a corrosive environment, neither of which when operating separately could cause major damage. A threshold stress is needed for crack initiation and growth, the level of which is normally well below that required to cause yielding. Specific corrosive environments can be quite mild, e.g. water vapour, although in the case of aluminium alloys it is common for halide ions to be present. The relative importance of each of the two factors, stress and corrosion (i.e. electrochemistry) varies with different ferrous or non-ferrous alloy systems. For aluminium alloys, there is general agreement that electrochemical factors predominate and it has been on this basis that new compositions and tempers have been developed which provide improved resistance to SCC (Section 3.5.5).

Only aluminium alloys that contain appreciable amounts of solute elements, notably copper, magnesium, silicon, zinc and lithium may be susceptible to SCC. When cracking does take place, it is characteristically intergranular (Fig. 2.20) and maximum susceptibility occurs in the recrystallized condition. For this reason compositions, working procedures and heat treatment temperatures for wrought alloys are normally adjusted to prevent recrystallization. It should be noted, however, that the resistance of a particular wrought alloy to SCC will now vary depending upon the direction of stressing with respect to the elongated grain structure. Maximum susceptibility occurs if stressing is normal to the grain direction, i.e. in the short transverse direction of components, because the crack path along grain boundaries is so clearly defined (Fig. 2.22).

Considerable effort has been directed towards understanding the mechanism of SCC in aluminium alloys and significance has been attached to the following microstructural features.

1. Precipitate-free zones adjacent to grain boundaries (Figs 2.7a and 2.12b)—in a corrosive medium, it is considered that either these zones or the grain boundaries will be anodic with respect to the grain centres. Moreover, strain is likely to be concentrated in the zones because they are relatively soft.
2. Nature of the matrix precipitate—maximum susceptibility to cracking occurs in alloys when GP zones are present. In this condition, deformation tends to be concentrated in discrete slip bands similar in appearance to those shown in Fig. 2.32a. It is considered that stress is generated where these bands impinge

upon grain boundaries which can contribute to intercrystalline cracking under stress-corrosion conditions (Fig. 2.12a).

3. Dispersion of precipitate particles in grain boundaries—in some aged aluminium alloys, it has been shown that SCC occurs more rapidly when particles in grain boundaries are closely spaced.
4. Solute concentrations in the region of grain boundaries—differences in solute levels that arise during ageing are thought to modify local electrochemical potentials. Moreover, it has been observed that a higher magnesium content develops in these regions. This results in an adjacent oxide layer with an increased MgO content which, in turn, is a less effective barrier against environmental influences.
5. Hydrogen embrittlement that may occur due to the rapid diffusion of hydrogen along grain boundaries.
6. Chemisorption of atom species at the surface of cracks which may lower the cohesive strength of the interatomic bonds in the region ahead of an advancing crack.

Recent experimental work has shown that stress-corrosion cracking at grain boundaries occurs in a brittle and discontinuous manner and there is clear evidence that hydrogen diffuses there, even in the absence of stress (e.g. Fig. 2.33). It thus seems that the presence of hydrogen does play a vital part in SCC due to one or both of mechanisms (5) and (6). However, the overall process of SCC is complex and it seems probable that one or more of the other microstructural factors

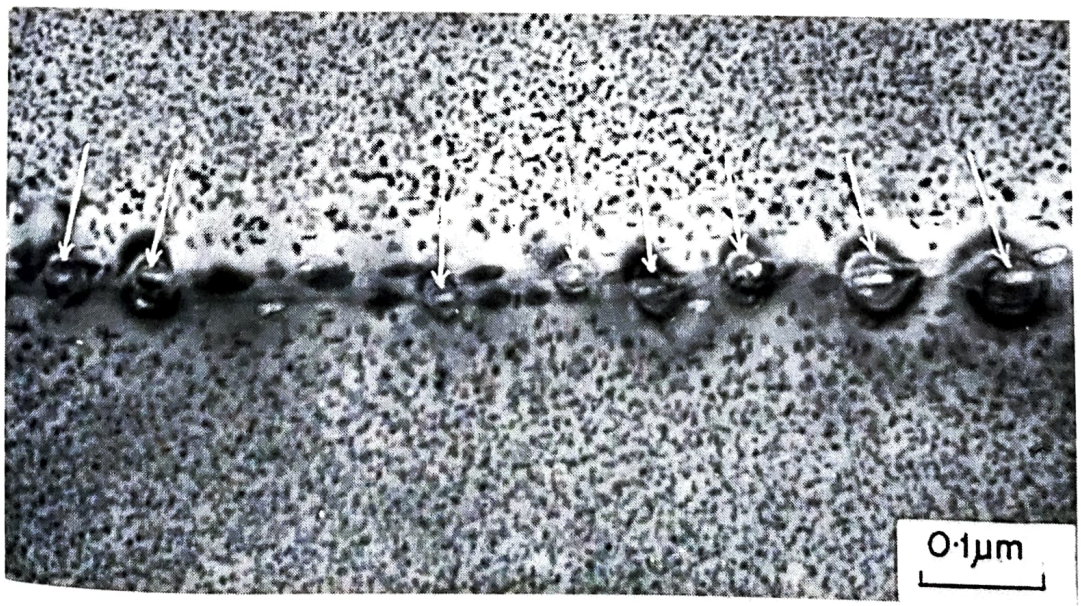

Fig. 2.33 Transmission electron micrograph showing hydrogen bubble development at precipitate particles in a grain boundary of a thin foil of an artificially aged Al–Zn–Mg alloy exposed to laboratory air for three months (from Scamans, G. M., *J. Mater. Sci.*, **13**, 27, 1978)

are also involved. The relative importance of each of these factors may depend upon the particular combination of alloy and environment.

2.4.5 Corrosion fatigue

Under conditions of simultaneous corrosion and cyclic stressing (corrosion fatigue), the reduction in strength is greater than the additive effects if each is considered either separately or alternately. Although it is often possible to provide adequate protection for metallic parts which are stressed under static conditions, most surface films (including naturally protective oxides) can be more easily broken or disrupted under cyclic loading.

In general, the reduction in a fatigue strength of a material in a particular corrosive medium will be related to the corrosion resistance of the material in that medium. Under conditions of corrosion fatigue all types of aluminium alloys exhibit about the same percentage reduction in strength when compared with their fatigue strength in air. For example, under freshwater conditions the fatigue strength at 10^8 cycles is about 60% of that in air, and in NaCl solutions it is normally between 25 and 35% of that in air. Another general observation is that the corrosion fatigue strength of a particular aluminium alloy appears to be virtually independent of its metallurgical condition.

2.4.6 Creep

Creep fracture, even in pure metals, normally occurs by the initiation of cracks in grain boundaries. The susceptibility of this region to cracking in age-hardened aluminium alloys is enhanced because the grains are harder and less willing to accommodate deformation than the relatively softer precipitate-free zones adjacent to the boundaries (Figs 2.7 and 2.12b). Moreover, the strength of the grain boundaries may be modified by the presence there of precipitate particles.

Precipitation-hardened alloys are normally aged at one or two temperatures which allow peak properties to be realized in a relatively short time. Continued exposure to these temperatures normally leads to rapid over-ageing and softening and it follows that service temperatures must be well below the final ageing temperature if a loss of strength due to over-ageing is to be minimized. For example, the alloy selected for the structure and skin of the supersonic Concorde aircraft, which is normally required to operate in service at 100–110°C, is aged at around 190°C.

Creep resistance in aluminium alloys is promoted by the presence of submicron intermetallic compounds such as Al_9FeNi or other fine particles that are stable at the required service temperatures (nor-